
Overcoming bias in representational similarity analysis

Roberto Viviani^{1,2}

1: Institute of Psychology, University of Innsbruck, Austria

2: Psychiatry and Psychotherapy Clinic III, University of Ulm, Germany

Roberto Viviani

University of Innsbruck

Institute of Psychology

Innrain 52

6020 Innsbruck, Austria

roberto.viviani@uibk.ac.at

Abstract

Representational similarity analysis (RSA) is a multivariate technique to investigate cortical representations of objects or constructs. While avoiding ill-posed matrix inversions that plague multivariate approaches in the presence of many outcome variables, it suffers from the confound arising from the non-orthogonality of the design matrix. Here, a partial correlation approach will be explored to adjust for this source of bias by partialling out this confound in the context of the searchlight method for functional imaging datasets. A formal analysis will show the existence of a dependency of this confound on the temporal correlation model of the sequential observations, motivating a data-driven approach that avoids the problem of misspecification of this model. However, where the autocorrelation locally diverges from its volume estimate, bias may be difficult to control for exactly, given the difficulties of estimating the precise form of the confound at each voxel. Application to real data shows the effectiveness of the partial correlation approach, suggesting the impact of local bias to be minor. However, where the control for bias locally fails, possible spurious associations with the similarity matrix of the stimuli may emerge. This limitation may be intrinsic to RSA applied to non-orthogonal designs. The software implementing the approach is made publicly available (<https://github.com/roberto-viviani/rsa-rsm.git>).

Overcoming bias in representational similarity analysis

Introduction

Representational similarity analysis (RSA, Kriegeskorte et al. 2008) is a multivariate technique to investigate cortical representations of objects or constructs defined by a set of properties (the stimuli, see also Edelman et al. 1998). A defining characteristic of this approach is that it eschews inversion of estimates of large covariance matrices, an ill-posed problem that easily gives rise to unstable estimates. Instead, RSA seeks evidence of cortical encoding of properties of stimuli by assessing the concordance between the matrix encoding the pairwise dissimilarity of stimuli and a matrix encoding the dissimilarity of the brain responses to the same stimuli (in an equivalent alternative formulation, which will be followed here, the concordance is based on measures of similarity). Combined with the searchlight approach (Kriegeskorte et al. 2006), RSA allows mapping the cortex to seek evidence for the representation of stimuli based on their properties as defined by the experimenter, usually in the context of functional imaging experiments.

A complication of functional imaging is that brain responses are not measured directly, but are mediated by the BOLD response. Hence, the brain signal to the presentation of a stimulus is estimated through the size of coefficients of a linear model encoding a canonical BOLD response. As it will be shown in detail below, a downside of RSA is that, unless the coefficients of this model were obtained with an orthogonal design, the covariance of these coefficients is confounded by the covariance arising from the design. Orthogonality is difficult to achieve because the sluggishness of the BOLD response introduces correlation between regressors of nearby trials. Because measures of similarity or dissimilarity between the brain signals are a function of their covariance, this confound contaminates RSA estimates. Cai et al. (2019) have drawn attention to this problem, and proposed a maximum-likelihood/Bayesian approach to overcome it. As in another related approach (Friston et al. 2019), this requires knowing the form of the covariance of the coefficients to model it parametrically. In contrast with this literature, the present work addresses the case when it cannot be assumed that the form of the covariance is known, also arguing based on two datasets that this case is a concrete possibility. Instead, it explores the effectiveness of estimating this covariance directly from the data of the whole volume and adjust for it using partial correlation. This approach is reminiscent of PET techniques of adjusting model coefficients for global signal levels, except that the global term here is a covariance, and adjustment takes place via partial correlation.

This paper is structured as follows. It will first be shown that a simple RSA estimator of similarity of the brain signal is biased, also tracing the connection between RSA and multivariate regression. This will lead to the rationale for the partial correlation approach, also justifying its use in the face of other possible approaches, such as whitening. The issue of estimating this confound in the setting of real EPI data will then be considered. Cai et al. (2019) found that their approach could not account for a small amount of residual bias.

It will be shown that small residual bias may arise from misidentifying the form of the autocorrelation of errors in the linear model, i.e. the lack of independence of sequential observations, as this model determines the covariance of the coefficients. We will explore the effectiveness of estimating this covariance from the volume data, and apply the proposed approach to two samples of real EPI data, one collected at ordinary and the other at short TRs (where lack of independence of sequential observations may be pronounced). The Discussion will mention the limitations of the RSA with the partial correlation approach, which are related to the difficulty of estimating the autocorrelation model accurately when it varies across the volume. The Material and Methods section will contain details on the acquisition parameters used in the MRI data.

The approach presented here was developed as an add-on function to the SPM package and is publicly available at <https://github.com/roberto-viviani/rsa-rsm.git>.

Results

Theory and simulations, ordinary least squares

When collected from a searchlight, the model may be written

$$\mathbf{Y} = \mathbf{X}\mathbf{B} + \mathbf{E},$$

where \mathbf{Y} is the n scans \times p searchlight voxels matrix of the imaging data, \mathbf{X} is a $n \times q$ design matrix usually containing q BOLD-convolved regressors for the signal elicited by the presentation of stimuli during the experiment, \mathbf{B} is a $q \times p$ matrix of coefficients to be estimated by least squares, and \mathbf{E} the $n \times p$ matrix of errors. This is the multivariate regression model, which is applied repeatedly to each searchlight; to simplify notation, indexes referring to the searchlight are omitted. It will also be initially assumed that the rows of \mathbf{E} be independent, an assumption that will be relaxed later. Well known results of multivariate regression are that the least squares estimates of \mathbf{B} are identical to those obtained by regressing on the individual columns of \mathbf{Y} separately (as in "the massively univariate approach" commonly adopted in functional imaging analyses), and that the expectation of these estimates and the expected variance-covariance are given by

$$E(\hat{\mathbf{B}}^V) = \mathbf{B}^V, \quad \text{Var}(\hat{\mathbf{B}}^V) = \boldsymbol{\Sigma} \otimes (\mathbf{X}'\mathbf{X})^{-1}. \quad (1)$$

In this expression, $E(\cdot)$ denotes expectation, $(\cdot)^V$ is the operator that stacks the columns of a matrix upon each other into a vector, $\boldsymbol{\Sigma}$ is the $p \times p$ variance-covariance of the columns of the errors (i.e., over voxels), and \otimes is the Kronecker product. From equation (1), the expected variance of a column $\hat{\boldsymbol{\beta}}_i$ of $\hat{\mathbf{B}}$ (the coefficient estimates from voxel i , $i = 1, \dots, p$) is

$$\text{Var}(\hat{\boldsymbol{\beta}}_i) = \sigma_i^2 (\mathbf{X}'\mathbf{X})^{-1}, \quad (2)$$

where σ_i^2 is the diagonal term of $\boldsymbol{\Sigma}$ giving the variance of the errors in voxel i (Mardia et al. 1979, pp. 160-161, 180-181).

After estimating the model coefficients $\hat{\boldsymbol{\beta}}_i$, RSA proceeds by selecting a set of coefficients or contrasts of coefficients for the analysis. Without loss of generality it will be assumed here that $\hat{\boldsymbol{\beta}}_i$ only refers to the required coefficients, usually obtained from a design in which the columns represent the expected BOLD response for each of the q stimulus presentations. At this point, there are several possible approaches to compute the similarity or dissimilarity matrix of the brain signal, but they have similar effects and are

all ultimately based on the inner product between the q rows of $\hat{\mathbf{B}}$, taken in pairs (Kriegeskorte and Diedrichsen 2019). In all approaches, encoding of the stimuli in the searchlight is assessed by the correlation between the off-diagonal terms of a matrix collecting these measures with those of the analogous matrix of the stimuli.

Here, the matrix $\hat{\mathbf{B}}\hat{\mathbf{B}}' = \sum_i \hat{\boldsymbol{\beta}}_i \hat{\boldsymbol{\beta}}_i'$ (the sum of squares and cross products of the coefficients) will be used, as it is the simplest expression of these inner products and leads to the simplest derivations. Generalization to other approaches is motivated later. Note that $\hat{\mathbf{B}}\hat{\mathbf{B}}'$ is not a sum of squares and cross-products matrix in the usual sense, because both columns and rows are not independent (as specified by $\boldsymbol{\Sigma}$ for columns and $(\mathbf{X}'\mathbf{X})^{-1}$ for rows in eq. 1).

Starting from these properties of the multivariate regression model, it may be shown (see the Appendix) that

$$E(\hat{\mathbf{B}}\hat{\mathbf{B}}') = \mathbf{B}\mathbf{B}' + \sum_i \text{Var}(\hat{\boldsymbol{\beta}}_i) \quad (3)$$

This result means that $\hat{\mathbf{B}}\hat{\mathbf{B}}'$ is a biased estimate of $\mathbf{B}\mathbf{B}'$, being confounded by $\sum_i \text{Var}(\hat{\boldsymbol{\beta}}_i) = \sum_i \sigma_i^2 (\mathbf{X}'\mathbf{X})^{-1}$ (see also Cai et al. 2019 for a related expression). RSA bias arises from an accidental correlation between the off-diagonal terms of the similarity matrix of the stimuli and those of $(\mathbf{X}'\mathbf{X})^{-1}$ unless the columns of \mathbf{X} are orthogonal and $(\mathbf{X}'\mathbf{X})^{-1} = \mathbf{I}$.

Note that the confound due to $\sum_i \text{Var}(\hat{\boldsymbol{\beta}}_i)$ is the same over all voxels and searchlights up to a multiplicative factor given by the voxel error variances σ_i^2 . Because also the similarity matrix of the stimuli is the same over all searchlights, this gives rise to a *global bias* whose intensity is modulated by the voxel error variances but has otherwise the same origin over the whole volume. In contrast, $\mathbf{B}\mathbf{B}'$ will usually vary between searchlights, and its off-diagonal terms will be correlated with the similarity matrix of stimuli only in few sparse areas. This suggests that the average RSA correlation from the searchlights over the whole volume may provide a rough but simple diagnostic for the existence of global bias (below, we refer to this diagnostic as the ‘average volume correlations’).

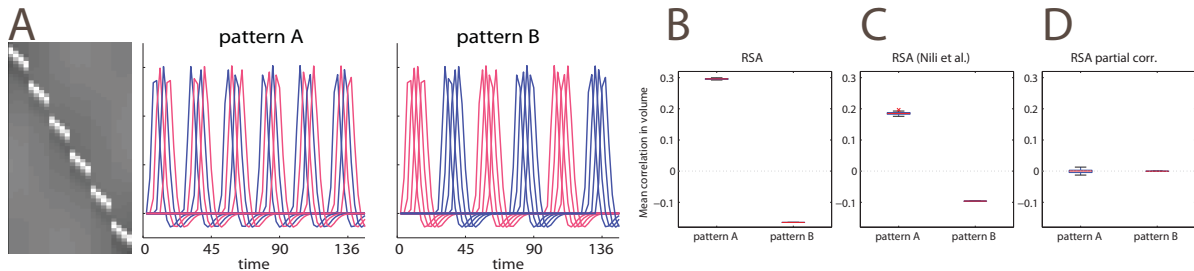


Figure 1. A: Schematic illustration of the design used to elicit bias in RSA. Design matrix (left) and classification of trials in two categories (shown in red and blue). This classification was chosen to produce correlation of coefficient models between trials of different categories (‘pattern A’, left) or between trials of the same category (‘pattern B’, right). B and C: RSA for patterns A and B in volumes containing white noise, boxplots of estimated average volume correlations (y axis). The boxplots show that these average correlations were very different from zero. The data in panel C were computed with the original RSA toolbox (Nili et al. 2014). D: average volume correlations of RSA conducted with the partial correlation approach, after partialling out the effect of $(\mathbf{X}'\mathbf{X})^{-1}$. One can see these correlations now being close to zero. s.d.: standard deviation.

The global bias arising from the non-orthogonality of the design is illustrated in Figure 1, assessed by the average volume correlations in simulated noise data with parameters comparable to those of a realistic MRI dataset and a design with strong non-orthogonality ($N = 30$; for details for the parameters used in the simulation, see the

Methods section). In panel A, BOLD-convolved regressors for trials modeling exposure to stimuli for three seconds are shown, grouped into 6 blocks of 4 trials each. The same stimuli are present in two patterns but in different arrangements. Pattern A comprised the stimuli of two different categories (in red and blue) alternating between trials within the blocks. In pattern B, the stimuli within the blocks belonged to the same category, in alternate blocks. While these designs may not be representative of those found in typical RSA studies, they provide a good challenge for the approaches to correct for the bias that follow. Figure 1B shows boxplots of the average volume correlations obtained by conducting a searchlight RSA of the similarity matrices of these two patterns after fitting the model to white noise data, where \mathbf{BB}' is zero. One can see from the boxplots that pattern A resulted in artificially inflated positive correlations, while pattern B produced the opposite effect. Bias was apparent also when using the original rsa toolbox (Nili et al. 2014), Figure 1C. The bias amount differs because of the different approach in assessing the concordance between brain signal and stimuli.

Several approaches are conceivable when forming the similarity or dissimilarity matrix of the brain signal (Kriegeskorte et al. 2008), but they all involve inner products (Kriegeskorte and Diedrichsen 2019) collected in the matrix of squares and cross-products of the model coefficients. In the approach of Nili et al. (2014), the brain activation pattern is captured by a correlation matrix with an inverted sign, and the concordance with the stimulus pattern is assessed with rank correlation. Relative to the sum of squares and cross products or a covariance matrix, correlation rescales the off-diagonal values, including those of $\sum_i \text{Var}(\hat{\beta}_i)$, however without taking them to zero. Using ranks in the correlation affects the efficiency of the measured associations, but does not abolish any accidental association with confound patterns.

Using a permutation strategy by randomly reassigning the category labels of trials to compute significance (Kriegeskorte et al. 2008) will not help addressing the issue of bias, because the trials are not exchangeable. Here, patterns A and B represent cases in which categories are ordered so as to capture the patterns induced by the design matrix best, albeit in different ways, giving correlations in opposite directions. Most permutations will deliver label patterns that are some mixture of patterns A and B, resulting in global bias values intermediate between those obtained with these two patterns. Hence, the correlations due to bias obtained with patterns A and B will be located at the far tails of the permutation distribution, mistakenly suggesting their significance even if they were computed from noise.

A perhaps natural approach to make $\sum_i \text{Var}(\hat{\beta}_i)$ diagonal would be to apply whitening. However, this approach will also represent the true similarity \mathbf{BB}' in the modified outer product, a consequence of whitening that requires attention. Here, applying a whitening matrix \mathbf{P} such that $\mathbf{P}^{\frac{1}{2}} \text{Var}(\beta_i) \mathbf{P}^{\frac{1}{2}} = \sigma_i^2 \mathbf{I}$ to both sides of eq. (3) will result in replacing \mathbf{BB}' with $\mathbf{P}^{\frac{1}{2}} \mathbf{BB}' \mathbf{P}^{\frac{1}{2}}$. The off-diagonal values of the whitened sum of squares and cross-products are now an unbiased estimator, but of $\mathbf{P}^{\frac{1}{2}} \mathbf{BB}' \mathbf{P}^{\frac{1}{2}}$, not \mathbf{BB}' . For example, if $\mathbf{BB}' = \mathbf{I}$, then the off-diagonal terms are those of \mathbf{P} .

To remedy the effects of the design covariance of regression coefficients on RSA, the approach explored here consists in partialling out the effects of $(\mathbf{X}'\mathbf{X})^{-1}$ on the off-diagonal terms of $\hat{\mathbf{B}}\hat{\mathbf{B}}'$ using partial correlation (i.e., using $(\mathbf{X}'\mathbf{X})^{-1}$ as a confound), instead of using simple correlation to test for the presence of the similarity pattern in $\hat{\mathbf{B}}\hat{\mathbf{B}}'$. An informal justification for this approach is that, in a linear model, estimates of coefficients

are unbiased irrespective of the amount of associations of predictors with possible confounds. We should therefore be able to retrieve unbiased estimates of association between $\mathbf{B}\mathbf{B}'$ and the similarity of stimuli irrespective of the accidental relation of these latter with $(\mathbf{X}'\mathbf{X})^{-1}$. The same may not be said for the whitening approach, as noted.

Figure 1D shows that this approach succeeds in taking the average volume RSA correlations to zero in the white noise data. In this simple case, this is almost a given, because the confound is exactly known up to the multiplicative factor of voxel error variance. This multiplicative factor is internally estimated by the partial correlation as the coefficient of the confound term in each searchlight separately. However, if this term is not known exactly, residual confounding may ensue. In the following, the issue of modelling the confound term is addressed for increasingly weaker assumptions.

Generalized least squares

The results so far were obtained under the simplifying assumption that the observations were independent. Most functional imaging analysis approaches reject this assumption and fit a generalized least squares model, for example by including a first-order autoregressive term \mathbf{G} estimated from residuals pooled over voxels,

$$\hat{\boldsymbol{\beta}}_i = (\mathbf{X}'\mathbf{G}^{-1}\mathbf{X})^{-1}\mathbf{X}'\mathbf{G}^{-1}\mathbf{y}_i.$$

The exact form of \mathbf{G} depends on the model for the temporal autocorrelation of residuals and on implementation details (in the SPM package used in the present work $\mathbf{G}^{-1} = \mathbf{V}^{-\frac{1}{2}}\mathbf{H}_0\mathbf{V}^{-\frac{1}{2}}$, where \mathbf{V} is an estimated AR(1) model for the residuals and \mathbf{H}_0 a residual-forming projection matrix implementing a high-pass filter). If this estimate is a good estimate of the true temporal dependency structure of the residuals, a standard result is that

$$\text{Var}(\hat{\boldsymbol{\beta}}_i) \approx \sigma_i^2(\mathbf{X}'\mathbf{G}^{-1}\mathbf{X})^{-1}, \quad (4)$$

which replaces the corresponding term in eq. (3). Note that temporal whitening at the first level model is not sufficient to abolish the confound arising from the design. On the contrary, now it is not certain that $\sum_i \text{Var}(\hat{\boldsymbol{\beta}}_i)$ is diagonal even if the columns of the design matrix were orthogonal to each other (this will also be the case for ordinary least squares if the data are filtered). To adjust for the effect of the design, in datasets where generalized least squares is used one may now use the off-diagonal terms of $\mathbf{Bcov} = (\mathbf{X}'\mathbf{G}^{-1}\mathbf{X})^{-1}$ to partial out its effects.

In practice, however, the autocorrelation model may not capture the true structure of the autocorrelation of the data. Furthermore, its estimate is usually computed from residuals pooled from multiple voxels, ignoring possible variations of the autocorrelation between voxels. Hence, a more realistic expression for the expected variance-covariance of the model coefficients may be given by

$$\text{Var}(\hat{\boldsymbol{\beta}}_i) = \sigma_i^2(\mathbf{X}'\mathbf{G}^{-1}\mathbf{X})^{-1}\mathbf{X}'\mathbf{G}^{-1}\boldsymbol{\Gamma}_i\mathbf{G}^{-1}\mathbf{X}(\mathbf{X}'\mathbf{G}^{-1}\mathbf{X})^{-1} \quad (5)$$

(Diggle et al. 2002, p. 60), where $\boldsymbol{\Gamma}_i$ is the true dependency of the errors in voxel i . Only if \mathbf{G} is a good estimate of $\boldsymbol{\Gamma}_i$ does this expression simplify to $\sigma_i^2(\mathbf{X}'\mathbf{G}^{-1}\mathbf{X})^{-1}$. This shows that, unless the autocorrelation term is appropriately modeled, residual confounding from the non-orthogonal design may still be present even after partialling out the effect of the off-diagonal terms of \mathbf{Bcov} . Unfortunately, appropriately modeling error dependencies may be an arduous task because the true structure of $\boldsymbol{\Gamma}_i$ is unknown (i.e, whether AR(1) or

something else) and may be influenced by study-specific factors (such as the properties of the MRI sequence, of the coil, and the frequencies of the regressors in the design matrix). As before, most terms of this expression are identical over the volume, inducing global bias, while the voxel-by-voxel variation of Γ_i introduces the possibility of *local bias*.

For the partial correlation approach, local bias means that one adjustment term alone may not control for the non-orthogonality of the design matrix satisfactorily. Nevertheless, even if \mathbf{G} is not a good approximation of Γ_i , it might be possible to address global bias by estimating the average variance-covariance $\text{V}\hat{\text{ar}}(\boldsymbol{\beta})_*$ from the whole volume:

$$\text{V}\hat{\text{ar}}(\boldsymbol{\beta})_* = \frac{1}{v} \sum_i (\hat{\boldsymbol{\beta}}_i - \bar{\boldsymbol{\beta}})(\hat{\boldsymbol{\beta}}_i - \bar{\boldsymbol{\beta}})', \quad \bar{\boldsymbol{\beta}} = \frac{1}{v} \sum_i \hat{\boldsymbol{\beta}}_i \quad (6)$$

Here, the asterisk in the subscript indicates that the variance-covariance is estimated from the whole volume (as opposed to any individual searchlight), and v is the number of voxels in the volume. One may then use the off-diagonal terms of $\mathbf{S}\text{var} = \text{V}\hat{\text{ar}}(\boldsymbol{\beta})_*$ in a partial correlation to control for global bias. The rationale for this approach is that global bias may be dominant given that most of the terms of eq. (5) are constant across the whole volume, and may be estimated as the average variance-covariance. A similar, even simpler approach consists of using the off-diagonal terms of $\mathbf{B}\mathbf{B} = v^{-1} \hat{\mathbf{B}}_* \hat{\mathbf{B}}_*'$ to control for global bias, where the asterisk in the subscript of $\hat{\mathbf{B}}_*$ indicates again that this is the matrix of the coefficients for the whole volume. $\mathbf{B}\mathbf{B}$ is confounded by the mean $\mathbf{B}\mathbf{B}'$ over the whole volume (eq. 3). However, since the local $\mathbf{B}\mathbf{B}'$ may be sparse and vary over searchlights, they may average out. With the due differences, use of $\mathbf{B}\mathbf{B}$ as confound is the closest equivalent of the ‘global covariate’ approach of PET analyses.

Partial correlation in EPI data

Global bias and its correction with partial correlation RSA was explored in real MRI data using the same design as in Figure 1A (Labek et al. 2017, $N = 27$, $\text{TR} = 2.27$ sec; for details, see the Methods section). The searchlight approach was used to seek artefactual evidence for representations of the fictitious patterns A and B (Figure 2).

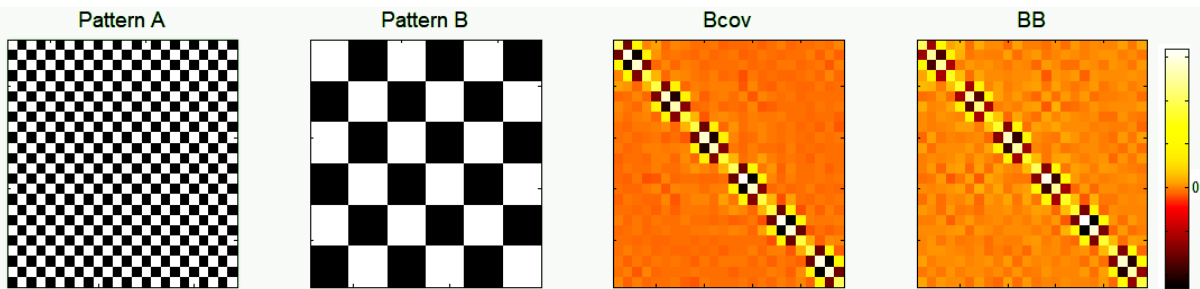


Figure 2. Similarity matrices for pattern A and B (left) and confound terms $\mathbf{B}\text{cov}$ and $\mathbf{B}\mathbf{B}$ (right) averaged over the whole sample. The data were here fitted with an AR(1) model for the temporal correlation of residuals. The first superdiagonal or subdiagonal from the main diagonal of $\mathbf{B}\text{cov}$ and $\mathbf{B}\mathbf{B}$ is similar to that of pattern A, while containing mostly values of the opposite sign than pattern B. The concentration of high absolute correlations near the main diagonal is due to the arrangement of the columns of the design matrix in the temporal order of the trials (shown in Figure 1A). $\mathbf{B}\mathbf{B}$, unlike $\mathbf{B}\text{cov}$, is computed without any knowledge of the design matrix. $\mathbf{S}\text{var}$, not shown here, has the same appearance as $\mathbf{B}\mathbf{B}$.

In Figure 3, panel A, global bias was assessed as in the simulations of Figure 1 by looking again at average volume correlations. There was evidence of global bias when

computing the representational analysis without partialling out any confound (ptn wo adjustment), similarly to the simulations conducted on noise data. In panel B, one can see second-level t maps of the RSA correlation for pattern A. The underlying average RSA volume correlations were positive in the whole volume, with peaks reaching $r = 0.15$, as one would expect in the presence of positive bias. This might not seem much, but the t map at the second level gave values ranging between 8 and 25 across the volume. These t values are high enough to cause rejection of the null hypothesis in all voxels in reasonable sample sizes.

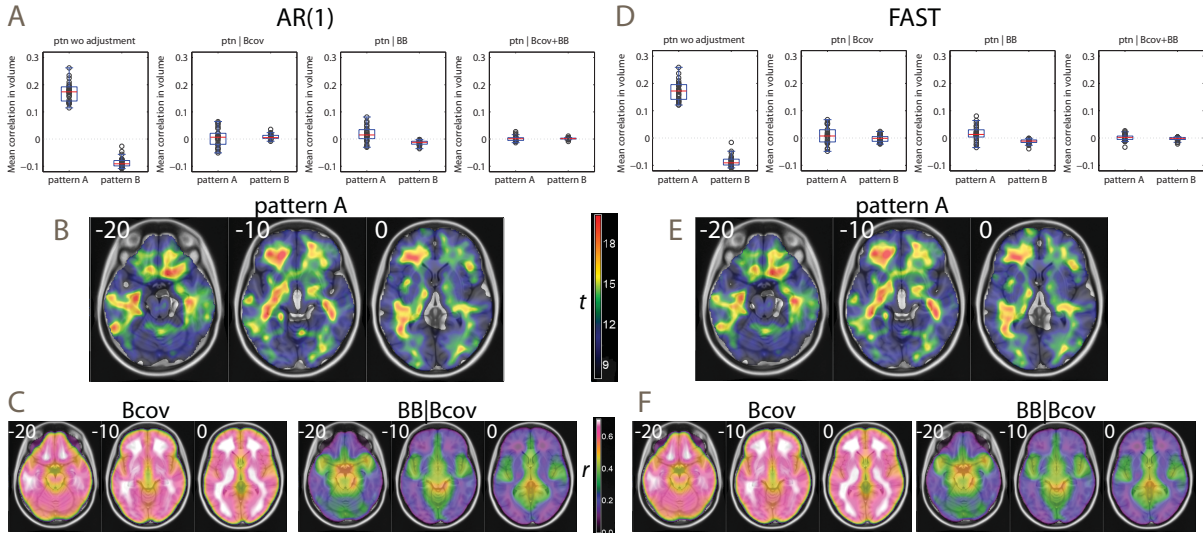


Figure 3. Analyses in real MRI data. Panels A-C: results obtained with an AR(1) for the lack of independence of sequential observations; panels D-F: same analyses obtained with FAST to model lack of independence. A and D: boxplots of mean volume correlations from the subjects in the sample. The boxplots on the left refer to RSA without partialling out confound terms; from second left to right, to RSA when partialling out **Bcov**, **BB**, and both for patterns A and B (cf. Figure 1). B, E: t maps of RSA correlations without correction, showing large artefactual positive correlations for pattern A. C, F: searchlight analysis of the RSA correlation of the confounds and the data.

The parametric maps of the artefactual correlations of pattern A, shown in Figure 3B, were positive over the whole volume but of varying local intensity. Recall that the term ‘global bias’ refers to the identical source of bias in the whole volume given by the theoretical covariance of the model coefficients **Bcov** of eq. (4), but the intensity of this bias may be locally modulated by residual variance and the relative magnitude of **BB'** in the individual searchlight. To assess its contribution, **Bcov** itself (as estimated from the AR(1) model of the pooled residuals by the SPM package) was used as a similarity map instead of pattern A in panel C, left. Similarly to the spatial distribution of the artefactual effect of pattern A, the spatial distribution of the effect of **Bcov** prevalently affected the white matter region. This is the behavior described in eq. (3) and (4), and may be understood by noting the similarity of the first superdiagonal of the similarity matrix of pattern A with that of **Bcov** (Figure 2). Inspection of the artefactual correlation for pattern B revealed a similar effect over white matter, but in the negative direction (not shown here for brevity).

The effectiveness of the partial correlation adjustments are shown in the remaining boxplots of panel A. Partialling out the off-diagonal terms of **Bcov** removed a large part of global bias (panel A, ptn|Bcov, second from left), as did using **BB** (ptn|BB, third from left), as shown by the average volume correlations being close to zero. Indeed, **Bcov** and **BB** were similar in these data (Figure 2). However, only using both **Bcov** and **BB**

simultaneously achieved results comparable to those of the simulations with noise (ptn|Bcov+BB, right), suggesting the existence of local bias (i.e., bias that could not be captured by one covariance term alone). Testing this latter RSA model using a permutation method to correct for multiple testing on leave-one-out resampling of the original data gave a false positive rate of 0.07 for $p < 0.05$.

To show where BB might have improved over Bcov in the combination, Panel C of Figure 3, right, displays the RSA of BB itself used as a similarity map after partialling out the effect of Bcov. The strongest correlations followed the distribution of vessel density (Viviani 2016), a main source of high variance in EPI data originating in blood pulsation (Lund et al. 2006). The increased signal on the midline is similar to effects of respiratory volumes reported by Birn et al. (2006). These voxels were missing from the RSA of Bcov, notwithstanding the high levels of signal noise, as one would expect if Bcov was less good as a model of the covariance of the coefficients in these voxels. There was no qualitative difference when using Svar instead of BB in these analyses.

In panels D-F of Figure 3 we repeated the same analyses using FAST (Corbin et al. 2018), an option in the SPM package to model autocorrelations more flexibly by including several exponential time terms and their derivatives. The results were similar to those of the AR(1) model, suggesting the simpler model to be adequate in this case.

A question raised by these data is whether the effectiveness of adjusting by Bcov may be due to the ease with which the autocorrelation of residuals is modelled in these data. In Figure 4 we applied the same partial RSA strategy to correct for global bias in MRI data collected for the present study with TR = 0.34 sec ($N = 32$), where the correlation of sequential acquisitions may be larger. Perhaps surprisingly, the extent of global bias was smaller here than in the previous sample. Nevertheless, there were widespread artefactual RSA correlations (panel B), following the spatial pattern of Bcov, which loaded above all on the center of the volume (where noise increases with distance from the coil) and to a lower extent on white matter (panel C). These findings are consistent with a much larger relative contribution of thermal noise in the variance of these data. The relative contribution of BB involved here gray matter. The control for global bias through partial correlation was equally effective as in the long TR data (panel A).

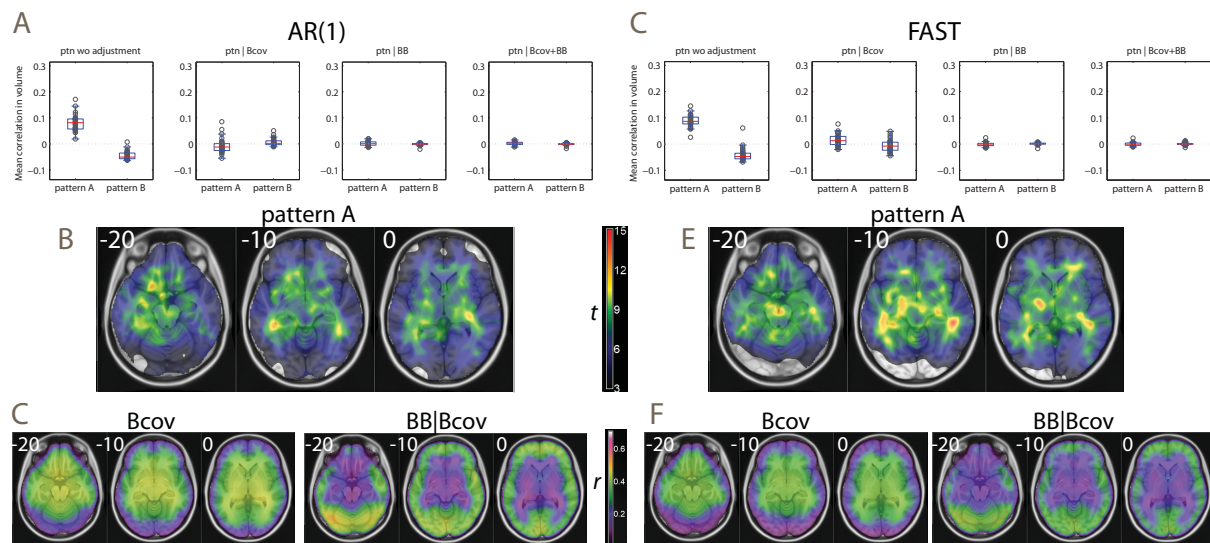


Figure 4. Analyses in real MRI data at short TR (same organization of panels as in Figure 3). Note that the scale of the t maps in B and E differs from the one used in Figure 2.

The use of FAST in this dataset (panels D-F) revealed the relative contribution of BB to be lower after adjusting for Bcov, as one would expect in a more realistic autocorrelation model of the error. However, we also observed high variation in the estimates of the autocorrelation term. There were no false positives in the leave-one-out resampling estimate of the FAST model after partialling out BB and Bcov at the $p < 0.05$ threshold, corrected at voxel level with the permutation method.

Additional strategies for the control of bias

Several additional strategies to control for bias are conceivable in individual studies. One is limiting the volume mask to gray matter to make the residual correlation model more representative of the target brain areas. A more aggressive strategy consists in computing correlations between off-diagonal terms further away from the main diagonal, as those close to it, if the regressors for the single coefficients were arranged in temporal order in the design matrix, are those where the effect of the design is strongest (Figure 2). This means omitting the cross-products of trials that are temporally close to each other in the statistics, assuming that similarity can be estimated from further trials. This strategy may be thought of as a resampling alternative to whitening: while this latter weights the coefficients of nearby trials to adjust for the estimated covariance, here these trials are simply omitted, obviating the need for an accurate estimate of this covariance. If stimulus presentations are distributed equally in nearby and in far trials, the estimates of concordance may be unbiased by the same reasoning that applies to estimates from ‘missing at random’ data. In our dataset, implementing this strategy improved uncorrected global bias (Figure 5). However, partial correlation still appeared to improve the level of global bias in individual volumes in these data. A possible explanation of this finding is that elements of Bcov, and even more of BB, that are far from the diagonal have small values but are not zero (see Figure 2).

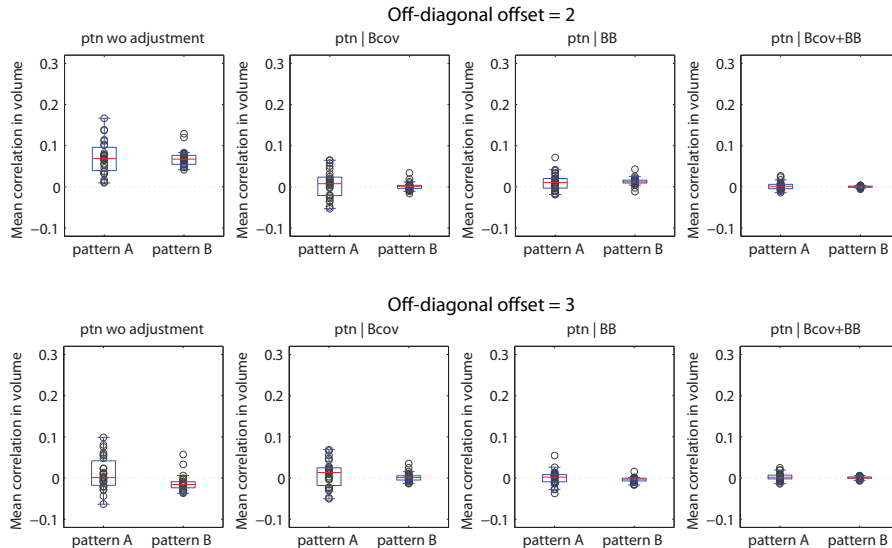


Figure 5. Average volume correlations estimates of global bias in the AR(1) model of long TR data when the sum of squares and cross products matrix is used with an off-diagonal offset of 2 and 3 units.

Discussion

This work sought to address the confound arising in RSA from the non-orthogonality of the design matrix using a partial correlation approach. Unfortunately, the precise form taken by the ensuing confound also depends on the temporal autocorrelation of the residuals in successive MR acquisitions, a quantity that is difficult to estimate. The importance of this issue in RSA contrasts with its benign consequences in ordinary

analyses of functional imaging experiments. Although the imaging literature contains numerous statements on the consequences of inadequate models of residual temporal correlation on correct significance levels, starting at least from Purdon and Weisskoff (1998), these consequences only concern inference at the first level (generalizing over scans within subjects), which is almost never considered in practice. Irrespective of residual correlations and how they are modelled, coefficient estimates (including OLS estimates) are always unbiased (Diggle et al. 2002), and in ordinary functional imaging studies it is these coefficient maps that are brought to the second level (to generalize over subjects), where they are independent. Hence, models of temporal autocorrelation in the ‘massively univariate’ approach of ordinary functional imaging studies only affect the efficiency of model estimates, not the correctness of inference at the second level. This fortunate state of affairs does not hold in RSA.

When the theoretical estimate of the covariance is adequate, its use as a confound term is straightforward. This is a pragmatic approach, but note that it has a justification in the unbiasedness of coefficients estimates in a linear model even when there is substantial association with confounds. When residual temporal autocorrelation is not adequately modelled, as appeared to be the case in our data, we explored the effectiveness of correcting for the ensuing global bias by estimating the covariance of the coefficients of the first-level model from the volume data and partialling it out. It is straightforward to increase the effectiveness of confound adjustment by adding different confound terms in the model and allow their effect to vary over the volume. These advantages are difficult to obtain with other strategies.

The use of covariance estimates of coefficients from volume data assumes that the association of the off-diagonal terms of \mathbf{BB}' and the stimuli similarity maps is present in few voxels, otherwise this association will be removed by the adjustment (Andersson et al. 2001). As in other global covariate approaches, if \mathbf{BB}' has the same form in large parts of the volume, the adjustment might introduce some bias of its own in place of the bias due to the design (Aguirre et al. 1998). This situation is essentially the same that confronts PET data analyses. It is even more difficult to provide a comprehensive strategy to counter local bias. The results presented here suggest that local bias was minor in our data, as shown by the large effects of corrections obtained with single terms, but it would be difficult to generalize to all possible datasets. Alternatively, the off-diagonal offset approach aims at obtaining estimates of concordance irrespective of what the covariance between nearby trials is by exploiting a weaker assumption of equal distribution of category labels in nearby and far trials. The price to pay is the exclusion of some trials from the analysis, reducing sensitivity.

It might be appropriate to compare the effect of different combinations of correction strategies and error correlation models, as true correlations with the similarity matrix of the stimuli should be robust to these variations. However, the possible existence of local bias implies no guarantee that the set of correction terms used be equally and uniformly effective in all voxels. In this case, possible spurious associations with the similarity matrix of the stimuli may emerge. This is an issue that may be difficult to address unless efficient methods to model the local model covariance of coefficients are developed.

It is important to underscore the fact that experimenters have recourse to planning the design so as to minimize the effects of the confound arising from the association from the model coefficients. It may also be possible to counteract bias by computing the

representational similarity analysis on chosen contrasts grouping trials so as to alter the extent of the association between the contrast coefficients, instead of using a design in which each trial is modelled by a single regressor. The design explored here was chosen because it considers the limit cases for positive and negative bias in the analysis, clarifying why bias may occur, not because it is representative of designs used in practice. In contrast, “condition-rich” designs are those thought best suited for representational similarity analysis, i.e. those with stimuli with many features (Kriegeskorte et al. 2008), whose accidental association with the pattern induced by the design may be less marked. However, application of RSA to the study of abstract features, such as those of high level cognition (Freund et al. 2021) might require modelling low-dimensional categories.

Methods

The study was based on the design of Labek et al. (2017), which was chosen because it used a classical block design giving rise to strong bias, and represents a limiting case where the bias is strong. Participants viewed drawings of individuals, each displayed for 3 sec. in blocks of 4 drawings. Hence, each block had a duration of 12 sec. Scrambled drawings were displayed between blocks for the same duration to form a high-level baseline. There were three blocks of drawings depicting sad individuals and three blocks of control drawings. Drawings and blocks were assigned to arbitrary stimuli classes to form the patterns of Figure 1. Both EPI samples were acquired on the premises of the Clinic for Psychiatry and Psychotherapy of the University of Ulm, Germany, after obtaining written informed consent from volunteers recruited locally. The study was approved by the Ethical Committee of the University of Ulm.

The simulations of Figure 1 were conducted in MATLAB. White noise volumes of isotropic voxel size 2mm were used as input data, creating 65 volumes for each of $N=30$ subjects. In the analysis of Figure 3, data were collected with a T2*-weighted EPI in a Siemens 3T Allegra scanner (TR/TE 2260/35 msec, flip angle 90°, in-planar voxel size 3x3mm, slice thickness 3mm, 25% gap between slices, 35 slices) with a single-channel head coil. In each of $N=27$ participants, 65 volumes were acquired. The data of Figure 4 were acquired in a Siemens 3T Prisma scanner with an EPI multiband sequence, with parameters chosen to minimize TR (slice acceleration factor 6, TR/TE 340/50 msec, flip angle 90°, in-planar voxel size 3x3mm, slice thickness 3mm, 13% gap between slices, 32 slices). No attempt was made to optimize for BOLD sensitivity, but we verified that the task and the contrast reported by Labek et al. (2017) were present in these data. Different pictures were used here for purposes extraneous to the present study. In each of $N=32$ participants, 433 images were acquired. To assist registration, a short T2-weighted EPI sequence of 5 volumes was acquired with no acceleration (TR/TE 4500/13 msec, flip angle 90°, same geometry as in the accelerated sequence). A 64-channels head coil was used with foam padding to minimize head motions.

The EPI data were preprocessed with SPM12 (Functional Imaging Laboratory, London), using standard procedures (realignment, normalization), producing data resampled at the isotropic voxel size 2mm. Normalization of the multiband data was based on multimodal segmentation, which included the mean multiband and the mean EPI without acceleration volumes simultaneously. The success of the segmentation was verified by inspection. Coefficients of noise and EPI data were modelled at the first level by convolving a stick function of duration 3 sec with a canonical BOLD curve. Each drawing presentation was modelled by its own regressor, giving as many beta images as

stimuli (as suggested by Kriegeskorte et al. 2008). An intercept and realignment parameters (when applicable) were added as confounding covariates. No high-pass filter or autocorrelation model was applied to noise data. The high-pass filter of EPI data was set at 128 sec. No smoothing was applied to volume data prior to computing the first level model.

The RSA was coded in MATLAB as an extension of the SPM package using the `spm_searchlight` function offered in that package. The spherical searchlight had a dimension of 8 mm, including 257 voxels when not located near the edge of the selected volume, defined by a mask including grey and white matter as well as CSF using the prior provided by SPM for these compartments at threshold $p < 0.5$. Searchlight volumes including less than 27 voxels were excluded. The similarity matrix contained the value zero for entries of different categories, and a constant value for entries of the same categories. As described in the main text, the similarity of the brain response was encoded as the sum of squares and cross products of the coefficients of the design shown in Figure 1. Pearson correlations and partial correlations between the upper diagonal terms of these two matrices were computed using the native MATLAB functions. BCOV was extracted from the internal SPM computation of that quantity, whereas SCOV and BB were computed as indicated by the equations in the main text. The results in Figure 1C were computed with the function `searchlightMapping_fmri` from the toolbox described by Nili et al. (2014), which uses Spearman correlation to assess correspondence.

The overlays of panels B and E of Figures 3 and 4 were obtained by computing t maps of one-sample t test of the searchlight correlations brought to the second level and smoothed with a Gaussian kernel (FWHM 4mm). The overlays of panels C and F are average maps of searchlight correlations (same smoothing). The false positive rates reported in text were computed by resampling the data without replacement, each time leaving out one individual at the second level, and computing significance levels with a permutation method for strong control of significance levels (percentiles of maximal t values over the volume, 2000 permutations per resampling; see Holmes et al. 1996). The rates are the percent of resamples where the null was rejected at the voxel level-corrected significance threshold $p < 0.05$.

Appendix

Recall that the least squares estimates of coefficients in the multivariate regression model $\mathbf{Y} = \mathbf{X}\mathbf{B} + \mathbf{E}$ are identical to those obtained by regressing on the individual columns of \mathbf{Y} separately (see the main text for notation). Considering the coefficients $\hat{\boldsymbol{\beta}}_i$ of the regressions on the individual columns of \mathbf{Y} , a standard result is the following,

$$\begin{aligned}\hat{\boldsymbol{\beta}}_i &= \boldsymbol{\beta}_i + (\mathbf{X}'\mathbf{X})^{-1} \mathbf{X}'\boldsymbol{\varepsilon}_i \\ &= \boldsymbol{\beta}_i + (\hat{\boldsymbol{\beta}}_i - \boldsymbol{\beta}_i)\end{aligned}$$

where $\boldsymbol{\varepsilon}_i$ is a column of \mathbf{E} (Mardia et al. 1979, pp. 160). Taking the squares of both sides of this equation and summing over the voxels indexed by i , one obtains

$$\sum_i \hat{\boldsymbol{\beta}}_i \hat{\boldsymbol{\beta}}_i' = \sum_i \boldsymbol{\beta}_i \boldsymbol{\beta}_i' + \sum_i (\hat{\boldsymbol{\beta}}_i - \boldsymbol{\beta}_i)(\hat{\boldsymbol{\beta}}_i - \boldsymbol{\beta}_i)' + \sum_i \boldsymbol{\beta}_i (\hat{\boldsymbol{\beta}}_i - \boldsymbol{\beta}_i)' + \sum_i (\hat{\boldsymbol{\beta}}_i - \boldsymbol{\beta}_i) \boldsymbol{\beta}_i'$$

When taking expectations, the cross-product terms $\sum_i \boldsymbol{\beta}_i (\hat{\boldsymbol{\beta}}_i - \boldsymbol{\beta}_i)' + \sum_i (\hat{\boldsymbol{\beta}}_i - \boldsymbol{\beta}_i) \boldsymbol{\beta}_i'$ vanish, giving

$$E(\hat{\mathbf{B}}\hat{\mathbf{B}}') = \mathbf{B}\mathbf{B}' + \sum_i \text{Var}(\hat{\boldsymbol{\beta}}_i).$$

Acknowledgments

This work was conducted within the framework of the “Austrian NeuroCloud”, supported by the Austrian Federal Ministry of Education, Science and Research. Acquisition of data was supported by a collaborative grant from the Federal Institute for Drugs and Medical Devices (BfArM, Bonn, Grant No. V-17568/68502/2017-2020).

References

- Aguirre, G.K., Zarahn, E., D'Esposito, M., 1998. The inferential impact of global signal covariates in functional neuroimaging analysis. *NeuroImage* 8, 302-306.
- Andersson, J.L., Ashburner, J., Friston, K., 2001. A global estimator unbiased by local changes. *NeuroImage* 13, 1193-1296.
- Birn, R.M., Diamond, J.B., Smith, M.A., Bandettini, P.A., 2006. Separating respiratory-variation-related fluctuations from neuronal-activity-related fluctuations in fMRI. *NeuroImage* 31, 1536-1548.
- Cai, M.B., Schuck, N.W., Pillow, J.W., Niv, Y., 2019. Representational structure of task structure? Bias in neural representational similarity analysis and a Bayesian method for reducing bias. *PLoS Comp. Biol.* 15(5), e1006299.
- Corbin, N., Todd, N., Friston, K.J., Callaghan, M.F., 2018. Accurate modeling of temporal correlations in rapidly sampled fMRI time series. *Hum. Br. Mapping* 39, 3882-3897.
- Diggle, P.J., Heagerty, P., Liang, K.Y., Zeger, S.L., 2002. *Analysis of Longitudinal Data* (2nd ed.). Oxford University Press, Oxford.
- Edelman, S., Grill-Spector, K., Kushnir, T., Malach, R., 1998. Toward direct visualization of the internal shape representation space by fMRI. *Psychobiol.* 26, 309-321.
- Freund, M.C., Etzel, J.A., Braver, T.S., 2021. Neural coding of cognitive control: The representational similarity analysis approach. *Trends Cogn. Sci.* 25, 622-638.
- Friston, K.J., Diedrichsen, J., Holmes, E., Zeidman, P., 2019. Variational representational similarity analysis. *NeuroImage* 201, 115986.
- Holmes, A.P., Blair, R.C., Watson, J.D.G., Ford, I., 1996. Nonparametric analysis of statistic images from functional mapping experiments. *J. Cereb. Blood Flow Metab.* 16, 7-22.
- Kriegeskorte, N., Diedrichsen, J., 2019. Peeling the onion of brain representations. *Annu. Rev. Neurosci.* 42, 407-432.
- Kriegeskorte, N., Goebel, R., Bandettini, P., 2006. Information-based functional brain mapping. *Proc. Natl Acad. Sci. USA* 103, 3863-3868.
- Kriegeskorte, N., Mur, M., Bandettini, P., 2008. Representational similarity analysis. Connecting the branches of systems neuroscience. *Frontiers Sys. Neurosci.* doi: 10.3389/neuro.06.004.2008.

- Labek, K., Berger, S., Buchheim, A., Bosch, J., Spohrs, J., Dommès, L., Beschoner, P., Stingl, J.C., Viviani, R., 2017. The iconography of mourning and its neural correlates: A functional neuroimaging study. *Soc. Cogn. Aff. Neurosci.* 12, 1303-1313.
- Lund, T.E., Madsen, K.H., Sidaros, K., Luo, W.-L., Nichols, T.E., 2006. Non-white noise in fMRI: Does modelling have an impact? *NeuroImage* 29, 54-66.
- Mardia, K.V., Kent, J.T., Bibby, J.M., 1979. *Multivariate Analysis*. Academic Press, London.
- Nili, H., Wingfield, C., Walther, A., Su, L., Marslen-Wilson, W., Kriegeskorte, N., 2014. A toolbox for representational similarity analysis. *PLoS Comp. Biol.* 10, e1003553. Software available at <https://www.mrc-cbu.cam.ac.uk/methods-and-resources/toolboxes/> (last visited 16 Sept. 2020).
- Purdon, P.L., Weiskoff, R.M., 1998. Effect of temporal autocorrelation due to physiological noise and stimulus paradigm on voxel-level false-positive rates in fMRI. *Hum. Br. Mapping* 6, 239-249.
- Viviani, R., 2016. A digital atlas of middle to large brain vessels and their relation to cortical and subcortical structures. *Frontiers Neuroanat.* 10, 12.